AD_____

Award Number: W81XWH-06-1-0315

TITLE: Revealing the Functions of Tenascin-C in 3-D Breast Cancer Models Using Cell Biological and In Silico Approaches

PRINCIPAL INVESTIGATOR: Agne Tarasevicuite

CONTRACTING ORGANIZATION: University of Pennsylvania
Philadelphia, PA 19104

REPORT DATE: March 2008

TYPE OF REPORT: Annual Summary

PREPARED FOR: U.S. Army Medical Research and Materiel Command
Fort Detrick, Maryland 21702-5012

DISTRIBUTION STATEMENT: Approved for Public Release;
Distribution Unlimited

REPORT DOCUMENTATION PAGE

Form Approved
OMB No. 0704-0188

1. REPORT DATE	2. REPORT TYPE	3. DATES COVERED
14-03-2008	Annual Summary	15 FEB 2007 - 14 FEB 2008

4. TITLE AND SUBTITLE
Revealing the Functions of Tenascin-C in 3-D Breast Cancer Models Using Cell Biological and In Silico Approaches

5a. CONTRACT NUMBER

5b. GRANT NUMBER
W81XWH-06-1-0315

5c. PROGRAM ELEMENT NUMBER

6. AUTHOR(S)
AGNE TARASEVICIUTE

Email: agnet@mail.med.upenn.edu

5d. PROJECT NUMBER

5e. TASK NUMBER

5f. WORK UNIT NUMBER

7. PERFORMING ORGANIZATION NAME(S) AND ADDRESS(ES)
University of Pennsylvania
Philadelphia, PA 19104

8. PERFORMING ORGANIZATION REPORT NUMBER

9. SPONSORING / MONITORING AGENCY NAME(S) AND ADDRESS(ES)
U.S. Army Medical Research and Materiel Command
Fort Detrick, Maryland 21702-5012

10. SPONSOR/MONITOR'S ACRONYM(S)

11. SPONSOR/MONITOR'S REPORT NUMBER(S)

12. DISTRIBUTION / AVAILABILITY STATEMENT
Approved for Public Release; Distribution Unlimited

13. SUPPLEMENTARY NOTES

14. ABSTRACT

See next page.

15. SUBJECT TERMS
ECM, Tenascin-C, Mammary Tissue Architecture, Stroma, Active Contours, 3-D Computational Modeling, c-met

16. SECURITY CLASSIFICATION OF:			17. LIMITATION OF ABSTRACT	18. NUMBER OF PAGES	19a. NAME OF RESPONSIBLE PERSON
a. REPORT	b. ABSTRACT	c. THIS PAGE			USAMRMC
U	U	U	UU	50	19b. TELEPHONE NUMBER *(include area code)*

14. Abstract
The extracellular matrix (ECM) glycoprotein tenascin-C (TN-C) is induced in the breast stroma, where it is associated with both breast cancer development and progression, yet its role in this disease remains obscure. To investigate the effects of stromal TN-C on normal human mammary epithelium, we cultured MCF-10A cells in a three-dimensional (3-D) reconstituted basement membrane (Matrigel), either with or without exogenous TN-C. Whereas control cells formed polarized acinar structures, complete with a continuous basement membrane and a central lumen (resulting from site-specific apoptosis), exposure to TN-C provoked selective loss of basement membrane and increased epithelial cell proliferation, without affecting apoptosis. To determine how these changes alter mammary epithelial tissue structure and function, an image analysis algorithm was developed to generate 3-D renditions of mammary acini, which were then used to assess and quantify acinar topography and volume. Although TN-C increased acinar surface roughness, it had no effect on volume. Based on these results, we hypothesized that TN-C promotes epithelial cell proliferation within the lumens of the acini, and that this process might involve c-met, a receptor tyrosine kinase which is over-expressed in breast tumors, where it is believed to affect both lumen formation and cell proliferation. Indeed, TN-C-treated acini contained filled lumens and expressed higher levels of c-met than controls. Furthermore, blockade of c-met resulted in reversion of the TN-C acinar phenotype, complete with restoration of acinar architecture, lumen formation and a decrease in proliferation that approached levels similar to those observed in controls. Importantly, human breast cancers enveloped by a TN-C-rich stroma expressed high levels of epithelial c-met when compared to normal tissue. Collectively, these 3-D studies indicate that TN-C compromises mammary epithelial tissue homeostasis via its effects on basement membrane integrity, c-met expression and luminal epithelial cell proliferation. These findings further support the notion that TN-C may be a suitable therapeutic target in breast cancer.

Table of Contents

Introduction

The extracellular matrix (ECM) glycoprotein tenascin-C (TN-C) has already been implicated in both breast cancer development and progression (Jones, 2001 & Jakhola, 1998). TN-C has also been independently linked to poor prognosis in breast cancer (Suwiwat, 2004). However, the mechanisms by which TN-C exerts its effects on human mammary epithelial cells within an appropriate tissue context have not been elucidated. The purpose of this training grant is to determine the mechanism by which TN-C perturbs normal tissue architecture in three-dimensional (3-D) organotypic cultures of human mammary epithelial cells by focusing on cell-cell junctions, as well as activation of receptor tyrosine kinases, namely c-met. Furthermore, as 3-D organotypic cultures are becoming more widely used in the biological community, we sought to develop a computational image analysis tool for objective evaluation of three-dimensional (3-D) architecture in organotypic cultures, in order to be able to determine the global effects of TN-C and other ECM components as well as oncogenes on overall tissue architecture. By elucidating the effects of TN-C on tissue architecture and gaining insights into the mechanisms involved, we hope to better understand how to rationally target the ECM, and TN-C in particular, for therapy in pre-malignant and malignant breast lesions.

Body

In task 1 we proposed to determine whether TN-C disrupts adherens junctions in normal mammary epithelial tissue structures. We initially carried out these experiments on two-dimensional (2-D) tissue culture plastic, where differences in the distribution pattern of β-catenin were noted upon culture in the presence of TN-C. Namely, there was increased accumulation of nuclear β-catenin and loss of β-catenin from the cell membrane. Upon closer inspection it became apparent that epithelial cells cultured in the presence of TN-C fail to 'zipper' together, creating gaps between the cells. It is likely that the mechanism for this involves tension forces generated on the actin cytoskeleton as well as the family of Rho GTPases, which controls the dynamics of the actin cytoskeleton. In fact, it has been shown that TN-C downregulates RhoA in fibroblasts, which may also provide an explanation for the lack of traction forces needed to bring epithelial cells close together (Midwood, 2002). These studies are currently being investigated in 3-D cultures. Briefly, normal human mammary epithelial cells (MCF-10A) are cultured in a reconstituted basement membrane in the presence or absence of TN-C. Whereas in the absence of TN-C, epithelial cells organize into spherical and smooth acinar structures, a high degree of dysmorphology is apparent when the cells are cultured in the presence of TN-C. Since some of the antibodies commonly used in 2-D are not suitable for immunofluorescent analysis in whole 3-D cultures, their expression patterns will have to be determined in frozen sections from 3-D cultures. These experiments are ongoing in order to determine whether loss of β-catenin from the cell membrane/disassociation of β-catenin/E-cadherin complexes and nuclear β-catenin accumulation also occur in the appropriate 3-D tissue context. To further investigate loss of β-catenin from the cell membrane, we conducted 2-D studies using substrate-bound TN-C to determine levels of associated E-cadherin/β-catenin as well as E-cadherin/α-catenin (another major component of adherens junctions) using immunoprecipitation (IP). We could not detect any differences in the levels of associated E-cadherin/β-catenin and E-cadherin/α-catenin in the presence or absence of TN-C. However, these were our findings in 2-D, and they do not necessarily suggest that the aforementioned associations between these proteins will be the same in 3-D cultures. One limitation of 3-D cultures is the amount of protein that can be retrieved from cells liberated from the surrounding basement membrane, and since large quantities of protein are required for IPs, it will be necessary to pool protein from 3-D cultures in order to obtain satisfactory quantities of protein for protein interaction analysis. At the moment, we have determined that the absolute minimum of protein required in order to detect E-cadherin/β-catenin and E-cadherin/α-catenin interactions is in the range of 100μg.
We are currently continuing to investigate the levels of cytoplasmic versus nuclear β-catenin in 3-D cultures, which will aid us in corroborating the IP studies for E-cadherin/β-catenin

interactions. We have already shown increases in nuclear levels of β-catenin on substrate-bound TN-C, albeit only in 2-D cultures thus far.

In task 2, we proposed to determine whether TN-C alters normal mammary tissue architecture by modulating the activity or distribution of the epidermal growth factor receptor (EGFR). We have conducted preliminary studies in 2-D cultures of normal human mammary epithelial (MCF-10A) cells and demonstrated the activation of the EGFR by Western immunoblotting in response to EGF present in MCF-10A growth medium. Since EGF is already a component of the growth and assay media, it is likely that the EGFR is always activated. Thus, it may not be feasible to explore whether TN-C increases the level of EGFR activation, or if it indeed maintains EGFR activation even upon withdrawal of EGF from (or blockade of EGF in) the growth medium. Thus, we have turned our attention to c-met, i.e. hepatocyte growth factor receptor (HGFR), another receptor tyrosine kinase that is modulated by TN-C in this 3-D system. We have demonstrated that TN-C significantly upregulates epithelial c-met levels (1.8-fold) in 3-D cultures, and that c-met blockade, using a function-blocking antibody, results in reversion of the TN-C phenotype, and decreases epithelial cell proliferation.

In task 3, we proposed to validate the effects of TN-C on mammary tissue architecture via AJ disruption and EGFR activation and/or distribution using a novel 3-D computer modeling approach. The computational modeling of 3-D mammary acini has been further developed in order to provide 3-D renditions of individual acini which can be compared to perfect ellipsoids (individual best-fitting ellipsoids for each acinus). This comparison has allowed us to derive an objective measure of the effects of TN-C on tissue architecture by measuring surface roughness, reported as the root mean square (RMS), derived from the difference in the Euclidian distance between the acinus and the ellipsoid. Upon analyzing 103 individual acini, we were able to objectively measure a 1.6-fold increase in surface roughness in 3-D mammary acini cultured in the presence of TN-C. Furthermore, it was also possible to calculate the acinar volume using 3-D acinar renditions, which revealed no difference in the presence or absence of TN-C. This finding, coupled with previous knowledge that proliferation of epithelial cells is increased in the presence of TN-C, while apoptosis is unaffected, suggested that the hyper-proliferating cells were accumulating within the lumens of the acini. We thus hypothesized that TN-C controls c-met, a receptor tyrosine kinase implicated in lumen formation and branching morphogenesis during mammary gland development (Tsarfaty, 1992) which is a proto-oncogene that is commonly upregulated in breast cancer (Lengyel, 2005). We have also preformed immunohistochemical analysis on human breast cancer tissue microarrays (n=80), which showed a strong correlation (60%) between TN-C-enriched stroma and epithelial c-met positivity.

Key Research Accomplishments

- TN-C increases epithelial cell proliferation in 3-D mammary epithelial cell cultures
- TN-C does not affect apoptosis in 3-D mammary epithelial cell cultures
- TN-C disrupts normal mammary epithelial tissue architecture
- Active contours-based computational argorithm developed
    - Surface roughness (RMS) measurements obtained for 103 acini
        - These measurements have allowed for objective assessment of 3-D tissue disorganization
        - TN-C increases surface roughness
    - Acinar volume measurements obtained
        - TN-C has no effect on acinar volume
- The computational information shed light on the mechanism for the actions of TN-C
    - The proto-oncogene c-met is implicated in luminal filling
    - TN-C upregulates c-met 1.8-fold, but not HGF
    - Stromal TN-C and epithelial c-met expression are highly correlated in human breast cancer tissues
    - c-met blockade reverts the TN-C phenotype

- Normalization of acinar architecture (decreased RMS values), normal lumen formation, decreased epithelial cell proliferation

Reportable Outcomes

Manuscripts:

1. Agne Taraseviciute, Benjamin Vincent & Peter Lloyd Jones "Quantitative analysis of 3-D human mammary epithelial tissue", re-submitted to American Journal of Pathology, March 2008.

Abstracts:

1. Agne Taraseviciute, Benjamin T. Vincent & Peter L. Jones. Stromal Tenascin-C in Breast Cancer: Effects on Mammary Epithelial Tissue Architecture. Western Student Medical Research Forum (WSMRF), February 2006.
2. Agne Taraseviciute, Benjamin T. Vincent & Peter L. Jones. Disruption of Normal Human Mammary Gland Architecture by Tenascin-C Revealed and Quantified Using an Active Contours-based Computational Model. Institute for Medicine and Engineering Symposium, May 2006.
3. Agne Taraseviciute, Kathryn Horwitz, Troy Stevens, Ilya Levental, Audra Goach-Sostarecz, Paul Janmey and Peter Lloyd Jones. Involvement of Macrovascular Tenascin-C in Breast Cancer Metastasis to the Lung. EMBO, June 2006.
4. Agne Taraseviciute, Kathryn Horwitz, Troy Stevens, Ilya Levental, Audra Goach-Sostarecz, Paul Janmey and Peter Lloyd Jones. Involvement of Tenascin-C in Mediating Breast Cancer Metastasis to the Lung: Effects on Endothelial Cell Surface Stiffness. ASCB, December 2006.
5. Agne Taraseviciute, Benjamin T. Vincent & Peter L. Jones. Stromal Tenascin-C Promotes Epithelial Cell Proliferation to Disrupt Normal Mammary Tissue Architecture at the Luminal Level. Gordon Research Conference on Mammary Gland Biology, June 2007.

Presentations:

1. Agne Taraseviciute, Benjamin T. Vincent & Peter L. Jones. Stromal Tenascin-C in Breast Cancer: Effects on Mammary Epithelial Tissue Architecture. Western Student Medical Research Forum (WSMRF), February 2006.

Conclusion

We have demonstrated that stromal TN-C disrupts normal mammary tissue architecture in 3-D organotypic cultures by increasing proliferation and upregulating c-met, ultimately leading to filled lumens within the acini. Furthermore, we have developed a computational image analysis tool which measures surface roughness and volume of mammary acini in order to quantify 3-D acinar architecture. This tool has allowed us to objectively measure the effects of TN-C in otherwise quite heterogeneous cultures. It also led us to hypothesize that luminal filling was occurring in TN-C-exposed cultures, since proliferation was increased, yet apoptosis and volume were unchanged. We were able to investigate the role of the receptor tyrosine kinase c-met in this process and subsequently showed that TN-C upregulates c-met. Thus, it was the findings obtained through computational biology that were informative for and paved the way for further investigations in cell biology. By uncovering the role for c-met, we were also able to block c-met function using an antibody approach, and thereby show reversion of the TN-C-induced acinar phenotype. Our understanding regarding how the extracellular matrix protein TN-C can perturb mammary tissue architecture has been advanced by revealing that the ECM can influence the oncogene c-met, and now we can begin to envision using a therapeutic approach to target the ECM and block the pathways involved in breast cancer pathogenesis.

References

Jones PL. Extracellular matrix and tenascin-C in pathogenesis of breast cancer. Lancet 2001;357(9273):1992-4.

Jahkola T, Toivonen T, Nordling S, von Smitten K, Virtanen I. Expression of tenascin-C in intraductal carcinoma of human breast: relationship to invasion. Eur J Cancer 1998;34(11):1687-92.

Lengyel E, Prechtel D, Resau JH, et al. C-Met overexpression in node-positive breast cancer identifies patients with poor clinical outcome independent of Her2/neu. Int J Cancer 2005;113(4):678-82.

Midwood KS, Schwarzbauer JE. Tenascin-C modulates matrix contraction via focal adhesion kinase- and Rho-mediated signaling pathways. Mol Biol Cell 2002;13(10):3601-13.

Suwiwat S, Ricciardelli C, Tammi R, et al. Expression of extracellular matrix components versican, chondroitin sulfate, tenascin, and hyaluronan, and their association with disease outcome in node-negative breast cancer. Clin Cancer Res 2004;10(7):2491-8.

Tsarfaty I, Resau JH, Rulong S, Keydar I, Faletto DL, Vande Woude GF. The met proto-oncogene receptor and lumen formation. Science 1992;257(5074):1258-61.

Appendices

Please find enclosed below a reprint of our manuscript submitted to American Journal of Pathology entitled “Quantitative analysis of 3-D human mammary epithelial tissue architecture reveals a role for tenascin-C in regulating c-met function”.

Quantitative analysis of 3-D human mammary epithelial tissue architecture reveals a role for tenascin-C in regulating c-met function

Agne Taraseviciute[1,4*], Benjamin T. Vincent[2*] & Peter Lloyd Jones[3,4†]

Department of Cell & Developmental Biology[1], University of Colorado at Denver & Health Sciences Center, Denver, CO 80262; Department of Psychology[2], University of Dundee, Dundee, DD1 4HN, UK; Department of Pathology & Laboratory Medicine[3], Institute for Medicine & Engineering[4], University of Pennsylvania, Philadelphia, PA 19104

* *Equal contribution*

†**Correspondence and reprint requests to:**
Peter Lloyd Jones, Ph.D.
University of Pennsylvania
1010 Vagelos Research Laboratories
3340 Smith Walk
Philadelphia, PA 19104-6383

Tel: 215-898-0048
Fax: 215-573-6815
e-mail: jonespl@mail.med.upenn.edu & b.t.vincent@dundee.ac.uk

text pgs: 35
tables: 2, # Figures: 6
Short running head (40 characters or less): Tenascin-C controls c-met function in 3-D
Grant #s & sources of support: This research was supported by a DOD pre-doctoral award to AT (BC050720), an EPSRC grant to BTV (GR/S47953/01(P)), and by University of Pennsylvania Academic Enrichment funds to PLJ.

Abstract

Remodeling of the stromal extracellular matrix (ECM) and elevated expression of specific proto-oncogenes within the adjacent epithelium represent cardinal features of breast cancer, yet how these events become integrated is not fully understood. To address this, we focused on tenascin-C (TN-C), a stromal ECM glycoprotein whose expression increases with disease severity. Initially, non-malignant human mammary epithelial cells (MCF-10A) were cultured within a reconstituted basement membrane (BM) where they formed 3-D polarized, growth-attenuated, multi-cellular acini, enveloped by a continuous endogenous BM. Upon addition of TN-C, however, acini failed to generate a normal BM, and net epithelial cell proliferation increased. To quantify how TN-C alters 3-D tissue architecture and function, we developed a computational image analysis algorithm, which showed that although TN-C disrupted acinar structure, it did not affect their volume. Thus, TN-C promoted epithelial cell proliferation within the acinar lumens, a process that we hypothesized involved c-met, a proto-oncogene amplified in breast tumors, that also causes intraluminal filling. Indeed, TN-C increased epithelial c-met expression and promoted luminal filling, whereas blockade of c-met function reversed this phenotype, resulting in normal BM deposition, lumen formation, decreased cell proliferation and restoration of acinar architecture. Collectively, these studies, combining a novel quantitative image analysis tool with 3-D organotypic cultures, demonstrate that stromal changes associated with breast cancer control proto-oncogene function.

Introduction

Most contemporary experimental and clinical breast cancer research studies have focused on the gain or loss of functions of oncogenes and tumor suppressor genes respectively as transforming events within the mammary epithelium[1]. However, equally compelling evidence demonstrates that the bio-chemical and -physical nature of the stromal extracellular matrix (ECM) microenvironment surrounding the epithelium also contributes to breast homeostasis and tumorigenesis[2, 3]. For example, when cultured within a laminin-enriched, compliant ECM, normal breast epithelial cells produce an endogenous basement membrane (BM), which directs the formation of polarized, spherical, multi-cellular acini, each of which contains a single, centrally-located lumen[4]. On the other hand, blocking over-exuberant β1 integrin signaling between malignant human breast cancer cells and their BM microenvironment induces phenotypic and functional normalization of mammary acini[5]. Conversely, ectopic overexpression of matrix metalloproteinase-3 (MMP-3) in the mouse mammary gland leads to chronic disruption of BM-derived signals, resulting in malignant behavior[6], as does increasing the biophysical stiffness of the normal stromal ECM[3]. Collectively, these and other studies reinforce the notion that tissue phenotype, specified by the ECM, can exert a dominant effect over the genotype of adjacent epithelial cells.

Three-dimensional (3-D) laminin-based cultures have allowed investigators to elucidate the effects of specific oncogenes on mammary epithelial tissue form and function in an appropriate, *in vivo*-like context. For instance, over-expression of ErbB2, or co-expression of cyclin D1 and the anti-apoptotic protein Bcl-2, in normal mammary epithelial cells generates a multi-acinar, hyper-proliferative phenotype characterized by luminal filling[7]. Mammary epithelial cells overexpressing either cyclin D1, or the HPV-16 E7 oncogene, however, form individual acini that possess normal lumens, but that are

of a greater size[8]. Therefore, different oncogenes exert distinct, site-specific effects on 3-D mammary acinar architecture and behavior. Given this, precisely determining how tumor-associated stromal ECM components alter 3-D tissue structure represents a key step in linking these changes to the activation or repression of specific genes and signaling pathways operating within the epithelium that elicit identical effects. Of course, this approach would rely upon the development of imaging tools that can accurately measure changes in mammary epithelial tissue structure within a pathobiologically-relevant 3-D microenvironment.

In this study, we devised a novel imaging tool to objectively measure how tenascin-C (TN-C), a stromal ECM glycoprotein induced in experimental and clinical breast cancer[9], affects normal human mammary epithelial 3-D tissue structure and function. In essence, we devised an algorithm to quantify acinar surface topography and volume in 3-D cultures of non-malignant human mammary epithelial (MCF-10A) cells interacting with TN-C. In this way, we discovered that in contrast to control cultures, those supplemented with TN-C possessed a disrupted endogenous BM, and an interior filled with proliferating epithelial cells. Since increased expression of the c-met proto-oncogene leads to intraluminal filling and cell proliferation[10], we hypothesized and thereafter demonstrated that c-met contributes to TN-C-dependent loss of normal mammary epithelial tissue architecture by affecting BM integrity, epithelial cell proliferation and lumen formation. Thus, the novel quantitative analyses of mammary epithelial tissue architecture presented herein provide a framework for understanding how the tumor stroma controls the function of a proto-oncogene that is amplified in human breast cancer.

Materials & Methods

Reagents

Cell culture medium (DMEM, F12/Ham's)), horse serum, 0.25% trypsin-EDTA and penicillin/streptomycin were from Invitrogen (Carlsbad, CA**).** Epidermal growth factor (EGF) was purchased from Peprotech (Rocky Hill, NJ). Cholera toxin, hydrocortisone, insulin and normal goat serum (NGS) were from Sigma-Aldrich (St. Louis, MO). Phenol Red-free, growth factor-reduced Matrigel was from BD Biosciences (San Jose, CA). Human TN-C protein was from Chemicon (Temecula, CA). Mouse-anti-human TN-C antibody was from Novocastra (Newcastle-upon-Tyne, UK). Laminin V (human-specific) and α6 integrin antibodies were from Chemicon, while Ki-67 and cleaved caspase-3 antibodies were from Zymed (Invitrogen; Carlsbad, CA) and Cell Signaling (Danvers, MA), respectively. c-met and HGF antibodies were from R&D Systems (Minneapolis, MN). Goat anti-mouse F(ab')$_2$ fragments were from Jackson ImmunoResearch (West Grove, PA). Donkey anti goat-HRP secondary antibody was from Santa Cruz Biotechnology (Santa Cruz, CA). All Alexa Fluor-conjugated (Alexa Fluor 488 and 594) secondary antibodies were from Molecular Probes (Invitrogen; Carlsbad, CA). 16% paraformaldehyde was from Electron Microscopy Sciences (Hatfield, PA). The Vectastain ABC and DAB kits, species-specific biotinylated secondary antibodies, and Vectashield mounting medium containing DAPI were from Vector Laboratories (Burlingame, CA). Cytoseal and Clear-Rite 3 were from Richard-Allan Scientific (Kalamazoo, MI). Pre-cast 4-20% precise protein gels were from Pierce (Rockford, IL).

Immunohistochemistry

Human breast tissue microarrays were from Ambion (Austin, TX), Cybrdi (Frederick, MD) and US Biomax (Rockville, MD). Pathologic diagnoses of tissue sections were

validated by an experienced pathologist. The histological profiles, ages and number of patients encompassed in the tissue microarrays are summarized in Table I. A pronase-based antigen retrieval process was used for TN-C immunohistochemistry, while citrate buffer was used for double immunostaining for TN-C and c-met. The primary antibodies were used at the following dilutions: TN-C at 1:50, c-met at 1:50. Sections were then incubated with biotinylated anti-mouse IgG (for TN-C), and biotinylated anti-goat IgG (for c-met) followed by the streptavidin/peroxidase ABComplex. The 3,3'-diaminobenzidine (DAB) chromogenic substrate was used to detect TN-C while the VectorNovaRED substrate was used to detect c-met. Sections were counter-stained with hematoxylin QS (for TN-C alone). For sections in which double-immunolabeling was performed, the streptavidin/alkaline phosphatase (AP) ABComplex was used, followed by the Vector Blue AP substrate. Sections co-immunostained for c-met and TN-C were mounted using Vectamount AQ. Images were captured using a Nikon 90i microscope equipped with a Nikon DXM1200 digital camera at 20X magnification (NA 0.75). TN-C immunoreactivity was scored blindly as low or high based on DAB staining intensity (Table II).

Three-Dimensional (3-D) Cell Culture

The MCF-10A nonmalignant human mammary epithelial cell line was obtained from the American Tissue Culture Collection (Manassas, VA). MCF-10A cells were maintained in DMEM/F12 medium containing horse serum (5%, Invitrogen, Carlsbad, CA**)**, supplemented with EGF (20 ng/ml; Peprotech, Rocky Hill, NJ), hydrocortisone (0.5 μg/ml), cholera toxin (100 ng/ml), insulin (10 μg/ml; all from Sigma-Aldrich, St. Louis, MO) and penicillin/streptomycin (1%) at 37°C and 5% CO_2. For 3-D cultures, an overlay method, originally developed by Bissell and colleagues[11, 12], was used. Briefly, cells

were trypsinized using 0.05% trypsin/0.53mM EDTA, re-suspended in assay medium (DMEM/F12, horse serum (2%), supplemented with EGF (10 ng/ml), hydrocortisone (0.5 μg/ml), cholera toxin (100 ng/ml), insulin (10 μg/ml) and penicillin/streptomycin (1%)) containing 2% Matrigel (phenol red-free, growth factor-reduced (BD Biosciences, San Jose, CA)) and plated on a solidified layer of Matrigel, either with or without purified human TN-C protein (10μg/ml; Chemicon, Temecula, CA). For c-met blockade studies, c-met antibody (R&D Systems, Minneapolis, MN) or goat IgG (Santa Cruz Biotechnology, Santa Cruz, CA) were used at 0.5-2μg/ml in both the solidified layer of Matrigel as well as in the overlay; the reported phenotypes and analyses were performed using the 1μg/ml concentration of the antibodies. Overlay assay medium was changed every 2-4 days and 3-D cultures were maintained for 4-8 days.

Immunocytochemistry

MCF-10A 3-D cultures (day 4 or day 8) were fixed in 3% paraformaldehyde, rinsed in 1X PBS, permeabilized in 1X PBS containing 0.5% Triton X-100 and stained according to standard methods using primary antibodies diluted in blocking solution (laminin V, 1:100; α6 integrin, 1:200; Ki-67, 1:50; cleaved caspase-3, 1:100; c-met, 1:50). This was followed by incubation in Alexa Fluor-conjugated species-specific secondary antibodies diluted in IF buffer (130mM NaCl, 7mM Na_2HPO_4, 3.5mM NaH_2PO_4, 7.7mM NaN_3, 0.1% bovine serum albumin, 0.2% Triton X-100, 0.05% Tween-20) containing 10% NGS (either Alexa Fluor 488 or 594 conjugated antibodies, 1:100). 3-D cultures were washed with IF Buffer and 1X PBS, and mounted with Vectashield medium containing 4',6 diamidino-2-phenylindole (DAPI). Z-stacks of images were obtained at 1 or 2 μm intervals using a Zeiss LSM 510 laser scanning confocal microscope (oil-immersion 25X objective, NA 0.8).

Nuclear Counts

Quantification of cellular proliferation (via Ki-67) and apoptosis (via cleaved caspase-3) was achieved using images obtained at 5 μm intervals from confocal Z-stacks of acini co-stained with DAPI. ImageJ software (http://rsb.info.nih.gov/ij/) was used to adjust color in the red, green and blue channels, achieve optimal brightness and contrast for the channel of interest, to convert image stacks to 8-bit files, to perform edge detection, and to threshold the images to delineate nuclei. Ki-67 or cleaved caspase-3 positive nuclei, as well as total nuclei (DAPI), were manually counted in thresholded image Z-stacks at 5 μm intervals. % Ki-67- or cleaved caspase-3-positive nuclei refers to the percent ratio of positive/total nuclei per individual acinus as measured for 17-100 acini per treatment condition.

Computational Biology

Image pre-processing

Z-stacks of confocal images derived from laminin V- or α6-integrin-immunostained acini were imported into Matlab (The MathWorks; Natick, MA), and stored as a 3-D matrix volume, $\mathbf{V} = \left(v_{i,j,k}\right)_{X\times Y\times Z}$, where there were Z-confocal slices each of resolution X×Y. Immunostaining intensity for a particular 3-D pixel (voxel) was thus described by $\boldsymbol{V}(i,j,k)$. These data were histogram normalized to the full range of intensity values 0-255, with the background staining intensity set to 0. A median filter was used to process each section of the Z-stack images (a particular value of k) in order to remove pixel noise.

Active contour optimization

To trace the edges of individual acini, the active surface was defined as a discrete set of points $S = s(p,q) = (x_{p,q},y_{p,q},z_{p,q})$[13], where each point in s represented a vector of length 3, containing its x, y, z coordinates. Here, s(*p,q*) represents a 2-D grid of points which is wrapped around to form a cylinder, *q* is the index for a slice number (corresponding to a specific confocal image slice at a particular *z*-depth), and there are ***Z*** slices in total. For each slice *q*, the active contour formed a 2-D outline consisting of *P* discrete points, typically in the order of 200. The active contour was constrained to be a cylinder by setting s(P*,q*) = s(*1,q*) (for all values of *q*). We did not constrain the active contour to be a closed sphere as the confocal data for the extreme polar regions of the acini was either too noisy or not present in order to allow for accurate fitting.

In order to fit the x, y, z positions of the active surface ***S*** to volumetric data ***V***, the equatorial section was manually traced in an approximate fashion (see Figure 2B, lower left panel). The equatorial slice was the only slice manually traced, which was subsequently optimized using the procedure described below. Briefly, all the remaining slices above and below the equatorial plane were sequentially and independently fit using the previous slice fit as the starting point. Active contour optimization was restricted in the z-axis as previously described due to limited resolution in the z dimension[14].

For any particular section, the contour was optimized using an iterative procedure to minimize the energy function, $E_{total} = E_{image} + E_{spacing}$. As with all active contour models, the final contour was balanced between low-level image and high-level shape properties. The low-level properties promoted points in the active contour to move toward regions of highest local immunostaining intensity. Optimization based solely on low-level features typically resulted in jagged and unsatisfactory contours which could get ‘caught’ or ‘snagged’ on highly stained debris. For this reason, high-

level features were also included and these took the form of prior knowledge regarding a certain degree of smoothness of the contour.

Low-level image features were calculated as $E_{image} = -w.G_\sigma * \left|\nabla \mathbf{V}(i,j,k)\right|$ in which G_σ was a 2-D Gaussian with standard deviation, σ. $\left|\nabla \mathbf{V}(i,j,k)\right|$ is the gradient of the immunostaining intensity $\mathbf{V}$ at the point **(*i*,*j*,*k*)** and w was used to set the relative importance of low-level image features. The dx, dy maps referred to below represent this gradient. High-level image features were defined by equal spacing of surface points in each section $E_{spacing} = \Sigma(d(a,b) - d(b,c))$, where $d(a,b)$ and $d(b,c)$ represented Euclidian distances between the contiguous points ab and bc respectively. In practice, $E_{spacing}$ was minimized by calculating a vector for each point directed toward the nearest point on the bisector of the two neighbouring points[15]. This approach resulted in $E_{spacing}$ = 0 when all points were equally spaced. By decreasing the value of w in E_{image}, the contribution of $E_{spacing}$ was increased, resulting in smoother fits.

A sequential technique for fitting the surface ***S*** to the acinar surface was employed. Initially, the entire surface was fitted using a larger Gaussian blur of the immunostaining intensity (typically σ = 6 pixels), which had the effect of smoothing over extraneous debris, and producing a good overall approximate fit after 400 iterations. A sequentially better fit was obtained by decreasing blur (smaller σ), calculating 400 iterations, and repeating until a minimum σ of 2 pixels was reached.

Morphological measures: Surface roughness (RMS), volume, and Mercator projections

A morphological measure was calculated based on the Euclidian difference between the 3-D surface of the acinus (delineated by the active mesh) and a best fitting ellipsoid model. The ellipsoid was chosen as an accurate representation of a smooth surface

which closely resembled the shape of spherical acini that became increasingly ellipsoidal upon squash introduced by coverslip placement. An ellipsoid, defined as $\frac{x^2}{a^2}+\frac{y^2}{b^2}+\frac{z^2}{c^2}=1$ where a,b,c are parameters defining the scale of the ellipsoid along each dimension, was fitted to the active surface using additional parameters to capture the center location, and orientation around the z-axis only. Best fitting ellipsoid parameters (one ellipsoid for each acinus) were calculated in spherical coordinates to minimize the root-mean-square (RMS) error between the ellipsoid and the acinar surface data. Obtaining a reliable surface roughness measure was clearly dependent upon the ellipsoid and so it was crucial to find the globally optimal ellipsoid parameters. To accomplish this, we optimised 100 separate ellipsoid models, each with different starting parameters. From these, the best fitting model was taken as a starting point and a further 100 estimates were produced, with slightly perturbed parameter values. The best fitting set of parameter values was chosen at this point. It was not possible in all cases to directly use the active surface to accurately measure acinar volume because polar regions of some acini were absent or noisy. We found estimation of acinar volume upon the ellipsoid fit which is given by $V=\frac{4}{3}\pi abc$ to be a satisfactory and consistent method, given the data at polar regions. Mercator projection maps were generated by plotting the difference between the acinar surface and the best ellipsoid model at each spherical coordinate. This effectively ‘unwraps’ the 3-D approximately spherical structure for easier visualization. Protrusions and indentations of different magnitudes of the acini are shown as positive and negative values, respectively, in the Mercator maps.

Western analysis

Cells were extracted from Matrigel using 1X PBS containing 0.5 mM EDTA, and lysed in 1X Cell Lysis Buffer (20mM Tris-HCl (pH 7.5), 150mM NaCl, 1mM EDTA, 1mM EGTA,

1% Triton X-100, 2.5 mM sodium pyrophosphate, 1mM β-glycerophosphate, 1mM sodium vanadate, 1μg/ml leupeptin) containing phosphatase and protease inhibitors. Conditioned medium (CM) was concentrated prior to western blotting. Cell lysates and CM were separated by SDS-PAGE on 4-20% gels (Pierce, Rockford, IL), transferred to PVDF membranes and probed with anti-c-met, -HGF, –GAPDH (Cell Signaling, Danvers, MA) or -β-actin (Sigma-Aldrich, St. Louis, MO) antibodies. HRP-conjugated secondary antibodies and ECL were used to visualize proteins using the Fuji LAS-3000 system. ImageGauge V4.22 software was utilized for densitometric quantification.

Statistics

Statistics were performed using an unpaired Student's t test. Error bars show standard error of the mean (SEM). Significant P values were <0.05 (* or **) where indicated. In cases where a sample size of n is indicated, n refers to the number of individual acini All experiments were performed at least in triplicate.

Results

TN-C promotes mammary epithelial cell proliferation & disrupts 3-D tissue organization

Immunohistochemical staining of human breast tissue microarrays, encompassing 427 individuals, showed that although TN-C was undetected in normal breast tissue (Figure 1A, top), it appeared at the stromal-epithelial interface in pre-malignant lesions, including ductal carcinoma *in situ* (DCIS; Figure 1A, middle), and at higher levels in the stroma of malignant breast lesions, including infiltrating ductal carcinoma (IDC) (Figure

1A, bottom). Elevated expression of stromal TN-C within tumors directly correlated with disease severity (Table II), and progressive loss of epithelial tissue architecture (Figure 1A). Whereas only 5-8% of normal, matched benign and carcinoma margin tissues expressed high levels of TN-C, strong stromal TN-C staining was evident in >50% of IDCs and 60% of metastases (Table II).

To determine whether TN-C directly affects the structure and function of the normal human mammary epithelium, TN-C-deficient MCF-10A cells were cultivated for 4 to 8 days in the presence of a reconstituted basement membrane (i.e. Matrigel), either with or without addition of exogenous, purified human TN-C protein. Although control and TN-C-treated cultures both formed 3-D acini, their gross appearance differed: control acini were mostly smooth and spherical, whereas acini exposed to TN-C were more disorganized (Figure 1B, left). To further assess these differences, we evaluated endogenous BM organization: whereas control acini were surrounded by a smooth, continuous, laminin-V-rich BM, this structure contained numerous gaps and folds when TN-C was present (Figure 1B, middle & right). In addition, epithelial cells appeared to be transiting through gaps in the BM into the surrounding TN-C-enriched microenvironment.

Since TN-C is known to support cell proliferation and survival in remodeling tissues[16], its ability to alter normal 3-D mammary epithelial tissue architecture may occur by increasing proliferation, and/or by decreasing apoptosis. Ki-67 immunostaining revealed a significant 1.6-fold increase in epithelial cell proliferation in response to TN-C (Figure 1B, middle & Figure 1C, left; 16.4 +/-2.0 versus 10.6 +/- 1.3; $p<0.009$). Levels of apoptosis within the acini, however, were identical in control and TN-C-treated cultures,

as determined by immunostaining for cleaved caspase-3 (Figure 1B, right & Figure 1C, right; -TN-C: 7.8 +/- 1.5, +TN-C 9.0 +/- 2.5, p=0.34).

TN-C affects acinar surface architecture, but not volume

Given that TN-C increases net epithelial cell proliferation, this might result in larger acini. Alternatively, increased proliferation may lead to intraluminal filling, without affecting volume. An objective assessment of these ideas is critical, since different cancer-associated genes are known to exert different effects at specific locations within 3-D mammary acini[17]. Nevertheless, although 3-D ECM-based cultures represent the current state-of-the-art method for examining cell behavior in an appropriate *in vivo*-like tissue context, they remain difficult to analyze due to their relatively large size and heterogeneous nature (Figure 1B, left). To redress this, we developed an image analysis tool to objectively quantify surface topographical features and volumes of 3-D mammary acini in mass culture. Surface roughness, evaluated by visualizing the endogenous BM, was chosen as an initial metric, because it is accepted that BM alterations not only reflect the state of tumorigenesis[18], but that perturbation or loss of this structure in and of itself may contribute to tumorigenesis[19].

To trace the exterior surface of mammary acini, an active contours-based algorithm was devised (Figure 2A). Individual 2-D image slices acquired at 1-2 μm intervals, as confocal Z-stacks of laminin-V or α6 integrin-stained acini, were used for this procedure. Next, the green channel in a 2-D equatorial plane confocal image was converted to an 8-bit grayscale image, and after noise removal, blurred image gradients (*dx* and *dy*) were obtained (Figure 2B, top). Subsequently, the active contour for the equatorial Z-plane was initiated by manually selecting numerous points close to the edge of the acini (Figure 2B, lower left), which were then automatically finalized, using

active contours, to create an accurate outline of the acinar edge (Figure 2B, lower right). This initial equatorial contour was then used as a reference point to automatically trace the remaining image slices in the Z-stack for each acinus, resulting in a montage of images (Figure 2C). Traced montages were then compared to the original images to check for gross errors in tracing, and each montage was then used to construct a 3-D rendition of each acinus (Figure 2D).

Using this method, we examined the effects of TN-C on tissue architecture in 103 individual 3-D acinar renditions generated in more than 3 independent experiments. Initially, surface roughness was measured by comparing the 3-D rendition to a customized, best-fitting ellipsoid, which represents a 'perfectly smooth' surface (Figure 3A). Even prior to calculating surface roughness, 3-D reconstructions of individual acini suggested that TN-C has a profound effect on normal mammary epithelial tissue architecture. Specifically, when compared to control cultures, numerous protrusions and indentations, reminiscent of branching structures, were apparent in acini cultured with TN-C (Figure 3A). Further analysis of these features confirmed that TN-C promotes a greater degree of radial deviation from the perfect ellipsoid when compared to a control (Figure 3B). To measure surface roughness in control and TN-C-treated acini, we calculated a root-mean-square (RMS) value based on the differences between Euclidian distances of 3-D acinar renditions versus a best-fitting ellipsoid. Smooth acini possessed lower RMS values, whereas dysmorphic acini produced higher RMS values (Figure 3C). TN-C-treated cultures exhibited a significant 1.7-fold increase in mean RMS value (RMS = 4.96±0.38), when compared to controls (RMS = 2.98±0.18, $p<0.001$). In addition to quantifying acinar surface roughness, additional features were explored. By 'unwrapping' 3-D renditions, Mercator projections were generated, permitting visualization of the finer surface features of control and TN-C-treated acini in

a topographical “map” format (Figure 3D). This analysis revealed that control acini possess a relatively “flat” surface landscape, whereas acini exposed to TN-C harbor numerous protrusions and indentations.

The distribution of RMS values and acinar volumes in both control and TN-C-treated conditions was then analyzed. Using logistic regression analysis, we calculated performance in terms of percent correct classification of a condition obtained via a bootstrap technique[20]. Using RMS measurements alone resulted in good discrimination performance of 69.8% ± 4.8 (Figure 4E, left), i.e. the control and TN-C-treated cultures were clearly separable into 2 populations. Taking volume measurements alone into account resulted in a lower performance of 56.6% ± 4.7 (Figure 4E, right), which was insufficient to separate the 2 populations. Thus, TN-C did not change acinar volume. However, upon taking both RMS and volume into account, the highest performance was obtained (Figure 4F) i.e. the control and TN-C-exposed acini could be segregated with approximately 80% accuracy. Thus, although TN-C had no significant effect on acinar volume, upon consideration of both volume and surface roughness, it became possible to predict the culture conditions of an individual acinus, i.e. whether they were cultured in the absence or presence of TN-C. Overall, since TN-C has no effect upon acinar volume, whilst increasing net cell proliferation, our quantitative analyses allowed us to hypothesize that stromal TN-C promotes epithelial cell proliferation leading to intraluminal filling.

TN-C promotes luminal filling by regulating c-met function

To test this hypothesis, we re-evaluated nuclear staining within acinar Z-stacks, which revealed that control acini possess a central lumen lined by a single layer of epithelial cells (Figure 4A, upper left), whereas TN-C-treated acini contained numerous lumens

lined by multiple cell layers (Figure 4A, upper right). Based upon these findings, we then explored the relationship between TN-C and c-met (i.e. the hepatocyte growth factor (HGF) receptor), a proto-oncogene that is amplified or overexpressed, but not mutated, in human breast cancer, where it is has been postulated to promote cell proliferation, migration and intraluminal filling[21]. Given these facts, we hypothesized that TN-C regulates c-met function to promote cell proliferation and subsequent intraluminal filling. Consistent with this, immunofluorescence staining of 3-D acini showed increased epithelial c-met levels in the presence of TN-C (Figure 4A, lower). Western immunoblotting supported these findings, revealing that TN-C significantly upregulates c-met expression 1.8-fold in 3-D cultures (Figure 4B & C), without affecting levels of secreted HGF (Figure 4B). Since HGF secretion is generally considered to be a hallmark of stromal cells, we also measured levels of HGF secretion in assay medium containing Matrigel in the absence of epithelial cells, and demonstrated that these levels are negligible (data not shown). Thus, MCF-10A epithelial cells do secrete HGF, thereby creating an autocrine signaling loop with c-met. Next, we co-immunostained breast cancer tissues for TN-C and c-met. In contrast to normal human breast tissue (Figure 4D, upper), TN-C was expressed within the stroma of a sub-set of IDCs that were also expressing c-met in the adjacent epithelial compartment (Figure 4D, lower).

Lastly, in order to determine whether the effects of TN-C on mammary tissue architecture are mediated by c-met, we inhibited c-met function in TN-C-treated 3-D mammary acini using a function-blocking antibody. When compared to controls, c-met blockade (at 1 μg/ml) reversed the TN-C phenotype, resulting in the formation of a continuous BM, accompanied by an ~50% decrease in epithelial cell proliferation, and generation of cleared lumens (Figure 5A & B). Furthermore, we quantified changes in acinar architecture upon c-met blockade, which demonstrate that RMS values are

decreased to control levels, supporting the notion that c-met blockade reverts the TN-C-induced phenotype (Figure 5C).

Discussion

Although it is fully accepted that alterations in the ECM microenvironment[19] and transformation of the adjacent epithelium by specific proto-oncogenes[1] contribute to cancer initiation and progression, how these events converge to impact overall normal breast epithelial structure and function is less well understood. Nevertheless, the novel quantitative image analysis procedure described herein allowed us to connect a pathologically-relevant breast cancer stromal component (i.e. TN-C) with the regulation and function of a proto-oncogene (i.e. c-met) that is known to be amplified in human breast cancer (Figure 6). Importantly, this method may now be applied to understand how other extrinsic factors control 3-D tissue organization and the expression or activity of genes and pathways already implicated in breast cancer, and how these events may become integrated.

TN-C is a multi-functional, context-dependent ECM component that has been postulated to contribute to pathological tissue remodeling via its ability to impact genome stability[22], cell cycle progression[23], production of MMPs[24], expression of vascular endothelial growth factor (VEGF)[25], as well as cross-modulation of receptor tyrosine kinases[9]. Even so, the precise manner in which TN-C controls mammary epithelial tissue behavior remained obscure. In this study, we not only show that TN-C regulates c-met, but that this event has functional consequences on both tissue form and function. Since TN-C and c-met have both been postulated to represent reliable markers for poor prognosis in breast cancer, these studies indicate that TN-C and its downstream effectors represent a potentially useful target in breast cancer treatment[26]. Consistent with this, TN-C radioimmuno-, RNAi- and aptamer-based strategies are already being evaluated at the clinical level for targeting malignant glioma and non-Hodgkins lymphoma[27-29], whereas growth and angiogenesis of human breast cancers in

a mouse tumour model are reduced using HGF and c-met antagonists[30,31].

In 3-D mammary epithelial cultures treated with TN-C, we recorded deficits in the production, assembly, and/or stability of the endogenous BM, as well as cellular trans-migration through this structure into the adjacent TN-C-enriched ECM. Analyses of various cells and tissues have also shown that TN-C protein is associated with a migratory phenotype *in vivo* and in culture. For example, activated focal adhesion kinase (FAK) promotes fibroblast migration via its ability to control TN-C expression at the transcriptional level[32]. Importantly, both FAK- and TN-C null mice exhibit migration and wound healing defects respectively [33,34] and *in vivo* knockdown of TN-C expression in avian embryos attenuates neural crest cell migration[35]. Once deposited in the ECM, TN-C may also control migration by disassembling stable focal adhesions[36], or by modulating the strength of cell binding interactions with other ECM molecules, including fibronectin (FN)[37], which is also induced in the breast tumor stroma[38]. As well, based upon our results, it is possible that TN-C promotes cell motility via induction of c-met, given that this protein appears to control this function in development and cancer[21].

It is plausible that TN-C disrupts endogenous BM by regulating the expression or activity of MMPs, an effect that has already been described for synovial fibroblasts, which produce increased levels of MMP-9 when interacting with mixed substrates of TN-C and FN[24]. However, gelatin substrate zymography did not reveal differences in MMP-9 levels or activity in response to TN-C (data not shown). Nonetheless, TN-C may stimulate MMPs that are not detectable via gelatin zymography, including MMP-12, which is upregulated by TN-C in 3-D cultures of gliomas[39], and MMP-3, which is activated in the involuting breast in concert with TN-C[40]. It is also possible that TN-C disrupts mammary epithelial tissue architecture in an MMP-independent manner through regulation of other ECM-degrading enzymes, such as the serine proteinase,

urokinase plasminogen activator, another reliable prognostic marker in breast cancer[41], and one that is expressed in the tumor stroma together with TN-C[42]. Alternatively, TN-C may lead to disruption of the BM in a protease-independent manner. For example, recent studies have shown that oral squamous cell carcinoma invasion and metastasis is associated with co-deposition of laminin-V and TN-C, and that these molecules form a physical complex[43]. Thus, TN-C may sterically interfere with normal BM deposition and function in tumors.

A central finding of this study is that TN-C promotes intraluminal filling of acini, a process that can occur when increases in cell proliferation are coupled with deficits in apoptosis within the acinar interior. For example, luminal filling has been noted when cyclin D1 is over expressed with the anti-apoptotic protein Bcl-2[17]. In our studies, however, apoptosis was not regulated by TN-C, suggesting that TN-C controls a different pathway involved in luminal filling. Accordingly, we focused on c-met, a proto-oncogene that is not only required for normal breast development[44], but also for increased cell proliferation, invasion through the ECM[45], and luminal filling[10]. Furthermore, and in common with TN-C, overexpression of c-met has been linked with poor prognosis and a high risk of metastasis[46]. At a histological level, c-met overexpression occurs in invasive ductal breast tumors bearing luminal aberrations[47], and activation of c-met by HGF has been shown to stimulate extensive development of branched structures by mammary epithelial cells cultured in 3-D[48]. Thus, it is plausible that TN-C-dependent induction of c-met promotes a branched phenotype, that may manifest itself in our system as increased surface roughness. In support of this idea, TN-C is expressed around the neck of the breast bud and portions of the branching ducts during mammary gland development[49]. Our findings are also consistent with recent reports which showed that overexpression of c-met in MCF-10A cells and in the

mouse mammary gland leads to increased branching and intraluminal filling, respectively[10,50]. Furthermore, a link between TN-C and c-met has been previously demonstrated in colon cancer-associated myofibroblasts, which secrete both TN-C and HGF, and have been shown to promote colon cancer cell invasion[51]. Mechanistically, c-met can collaborate with c-myc in promoting breast adenocarcinomas[10]**.** This finding may be relevant in the context of the present findings, because TN-C induces c-myc expression in 3-D cultures of quiescent mouse mammary epithelial cells[23]. Thus, evidence for the control of proto-oncogene expression by TN-C exists, albeit in a mouse model of mammary gland involution studying apoptosis. Additional studies will focus on how TN-C regulates c-met expression in the human mammary epithelium, and whether it also controls other pathways that collaborate with c-met. To this end, we have recently discovered that c-met forms a complex with activated epidermal growth factor receptors (EGFRs) in 2-D cultures of MCF-10A cells (Taraseviciute & Jones, unpublished). Since TN-C potentiates the activity of EGFRs[52], and EGFRs cross-modulate c-met activity[53], it is plausible that TN-C not only upregulates c-met expression, but that it indirectly controls its activity via interactions with EGFRs.

In summary, the combined use of a sophisticated 3-D organotypic culture system with a novel computational image analysis tool has allowed us to objectively measure how TN-C compromises human mammary epithelial tissue structure, gene expression and function. Above all, these studies reinforce the idea that microenvironmental cues originating within the tumor stroma can act in both a dominant and paracrine fashion to control the expression and function of epithelial genes already associated with the development and progression of breast cancer.

Acknowledgements

The authors wish to thank members of the Jones lab, the IME, Paul Jedlicka for providing pathology expertise regarding the pathological diagnoses in human breast tissue microarrays, Roland Baddeley and Eleanor Martin for their helpful comments.

Figure & Table Legends

Table I. Summary of breast tissue histology, patient age, and number of patients

Figure 1. Stromal TN-C alters normal 3-D mammary epithelial tissue architecture **(A)** Tissue sections from normal human mammary gland (top), DCIS (middle), and IDC (lower) stained with H&E (left) or TN-C (right). *Scale bar, 50mm.* **(B)** Morphology of MCF-10A acini generated in Matrigel, in the absence (top) or presence (lower) of TN-C for 8 days (left). Confocal immunofluorescence staining for laminin-V (green; middle and right), Ki-67 (red; middle) and cleaved caspase-3 (red; right) in 8 day cultures. Stars indicate loss of a continuous BM (middle) and transmigrating cells (right) in the presence of TN-C. *Scale bars, 50μm*. **(C)** Quantification of Ki-67 immunoreactivity in MCF-10A acini revealed a 1.6-fold increase in proliferation (n=66 acini; *p<0.009), yet no differences in apoptosis (quantification of cleaved caspase-3 immunoreactivity) in response to TN-C (n=40 acini; p=0.68).

Table II. Stromal TN-C intensity in normal, matched benign, malignant breast lesions and metastases.

Figure 2. Reconstructing 3-D mammary epithelial tissue architecture **(A)** Schema delineating the computational procedures used to measure acinar surface roughness and volume. **(B)** The equatorial 2-D confocal slice from a laminin-V immunostained acinus-in this example, derived from a TN-C-treated 8 day acinus-was subjected to *dx* and *dy* pre-processing based on fluorescence intensity (top). Active contours were manually initiated by selecting multiple points close to the edge of the acinus (lower left). After active contour fitting, a final trace of the edge was obtained automatically

(lower right). **(C)** The trace obtained in (B) was extrapolated to all subsequent remaining 2-D slices of the acinus resulting in a montage of traces. **(D)** Montages described in (C) were used to render a 3-D projection.

Figure 3. TN-C increases surface roughness, but not acinar volume **(A)** Examples of 3-D renditions of individual acini (black), generated in the absence (top) or presence (lower) of TN-C for 8 days. A customized ellipsoid (red-yellow) was designed and fitted to each individual acinus. **(B)** Change in radius for each acinar slice (black) denotes distance away from the perfect ellipsoid for the acini depicted in (A); the red horizontal line at '0' represents the perfect ellipsoid. In the absence of TN-C (top), each slice did not deviate more than a few μm from the perfect ellipsoid, whereas in the presence of TN-C (lower), deviations exceeded 10 μm. **(C)** 3-D acinar structure was quantified by measuring root mean square (RMS; absolute difference from perfect ellipsoid) values for acini cultured for 8 days in the absence or presence of TN-C. TN-C evoked a 1.7-fold increase in RMS (n=103; p=0.024). **(D)** Mercator projections of 3-D acini: protrusions are displayed in yellow and red while indentations appear blue. **(E)** Distribution of RMS values (left) and volumes (right) for acini generated in the absence (dashed line) or presence (solid line) of TN-C for 8 days. **(F)** Plotting RMS versus volume yields 2 distinct groups of acini with the line showing the best linear classification using logistic regression at a performance of 79.5%.

Figure 4. TN-C promotes luminal filling and upregulates c-met **(A)** Confocal immunofluorescence staining for laminin-V (green; upper) and nuclei (blue) revealed changes in lumen structure (white dotted lines) in acini cultured with or without TN-C. C-met staining intensity is increased in the presence of TN-C (lower right) when compared

to control (lower left). *Scale bars, upper panels, 50μm; lower panels, 25 μm.* **(B)** Western blot analysis confirmed that c-met levels are increased in the presence of TN-C, while secreted HGF levels remain unchanged. GAPDH is the loading control. **(C)** Densitometric analyses of c-met levels relative to GAPDH or β-actin reveal a significant 1.8-fold increase in the presence of TN-C. **(D)** Tissue sections from the normal human mammary gland (top) and grade 2 IDCs (middle and lower) stained with H&E (left) or c-met and TN-C (red and blue respectively; right). *Scale bar, 50μm*.

Figure 5. Blocking c-met function reverses the TN-C-dependent phenotype **(A)** Phase contrast (top) and confocal immunofluorescence (lower) photomicrographs shows normalization of the TN-C-induced phenotype upon introduction of a function-blocking c-met antibody. **(B)** C-met blockade significantly decreases the proliferation of MCF-10A acini treated with TN-C (-TN-C + IgG, 1.0 +/- 0.07; +TN-C + IgG, 1.33 +/- 0.08; +TN-C + α-c-met, 0.35 +/-0.06; n=100; *p=0.0018; **p=0.000014).

Figure 6. Hypothetical schema delineating how TN-C promotes intraluminal filling via c-

met

Histological type	Age range (mean)	Number of patients
Atypical lobular hyperplasia	60-67 (63.5)	2
Ductal carcinoma *in situ* (DCIS)	29-81 (49.5)	6
Epithelial hyperplasia	48	1
Infiltrating ductal carcinoma (IDC)	24-88 (55)	200
Lobular carcinoma	55	1
Margin of carcinoma	31-74 (49.4)	29
Matched benign	21-88 (54)	25
Medullary carcinoma	52-55 (53.5)	2
Metastatic adenocarcinoma	40-95 (63.9)	20
Mucinous adenocarcinoma	39-53 (46.3)	4
Normal breast tissue	18-96 (47.1)	128
Paget's disease	37-51 (46)	4
Papillary carcinoma	48-77 (64)	3
Squamous epithelium of the nipple	44	1
Tubular carcinoma	41	1
Total	18-95 (52.4)	427

Table I

Histological type	Low TN-C expression (number (%))	High TN-C expression (number (%))	Number of patients
Infiltrating ductal carcinoma	96 (48)	104 (52)*	200
Margin of carcinoma	27 (93)	2 (7)	29
Matched benign	23 (92)	2 (8)	25
Metastastic breast carcinoma	8 (40)	12 (60)*	20
Normal breast tissue	121 (95)	6 (5)*	127

Table II

References

1. Hanahan D, Weinberg RA: The hallmarks of cancer, Cell 2000, 100:57-70
2. Bissell MJ, Radisky D: Putting tumours in context, Nat Rev Cancer 2001, 1:46-54

3. Paszek MJ, Zahir N, Johnson KR, Lakins JN, Rozenberg GI, Gefen A, Reinhart-King CA, Margulies SS, Dembo M, Boettiger D, Hammer DA, Weaver VM: Tensional homeostasis and the malignant phenotype, Cancer Cell 2005, 8:241-254

4. Aggeler J, Ward J, Blackie LM, Barcellos-Hoff MH, Streuli CH, Bissell MJ: Cytodifferentiation of mouse mammary epithelial cells cultured on a reconstituted basement membrane reveals striking similarities to development in vivo, J Cell Sci 1991, 99 (Pt 2):407-417

5. Weaver VM, Petersen OW, Wang F, Larabell CA, Briand P, Damsky C, Bissell MJ: Reversion of the malignant phenotype of human breast cells in three-dimensional culture and in vivo by integrin blocking antibodies, J Cell Biol 1997, 137:231-245

6. Sternlicht MD, Lochter A, Sympson CJ, Huey B, Rougier JP, Gray JW, Pinkel D, Bissell MJ, Werb Z: The stromal proteinase MMP3/stromelysin-1 promotes mammary carcinogenesis, Cell 1999, 98:137-146

7. Slamon DJ, Godolphin W, Jones LA, Holt JA, Wong SG, Keith DE, Levin WJ, Stuart SG, Udove J, Ullrich A, et al.: Studies of the HER-2/neu proto-oncogene in human breast and ovarian cancer, Science 1989, 244:707-712

8. Debnath J, Mills KR, Collins NL, Reginato MJ, Muthuswamy SK, Brugge JS: The role of apoptosis in creating and maintaining luminal space within normal and oncogene-expressing mammary acini, Cell 2002, 111:29-40

9. Jones PL: Extracellular matrix and tenascin-C in pathogenesis of breast cancer, Lancet 2001, 357:1992-1994

10. Welm AL, Kim S, Welm BE, Bishop JM: MET and MYC cooperate in mammary tumorigenesis, Proc Natl Acad Sci U S A 2005, 102:4324-4329

11. Debnath J, Muthuswamy SK, Brugge JS: Morphogenesis and oncogenesis of MCF-10A mammary epithelial acini grown in three-dimensional basement membrane cultures, Methods 2003, 30:256-268

12. Li ML, Aggeler J, Farson DA, Hatier C, Hassell J, Bissell MJ: Influence of a reconstituted basement membrane and its components on casein gene expression and secretion in mouse mammary epithelial cells, Proc Natl Acad Sci U S A 1987, 84:136-140

13. Takanashi I, Muraki S, Doi A, Kaufman A: Three-dimensional active net for volume extraction. Edited by San Jose, CA, USA, SPIE-Int. Soc. Opt. Eng, 1998, p.184-193

14. Cohen LD, Cohen I: Finite-element methods for active contour models and balloons for 2-D and 3-D images, IEEE Transactions on Pattern Analysis and Machine Intelligence 1993, 15:1131-1147

15. Perrin DP, Smith CE: Rethinking classical internal forces for active contour models. Edited by Kauai, HI, USA, IEEE Comput. Soc, 2001, p.615-620

16. Jones FS, Jones PL: The tenascin family of ECM glycoproteins: structure, function, and regulation during embryonic development and tissue remodeling, Dev Dyn 2000, 218:235-259

17. Reginato MJ, Mills KR, Becker EB, Lynch DK, Bonni A, Muthuswamy SK, Brugge JS: Bim regulation of lumen formation in cultured mammary epithelial acini is targeted by oncogenes, Mol Cell Biol 2005, 25:4591-4601

18. Petersen OW, Ronnov-Jessen L, Howlett AR, Bissell MJ: Interaction with basement membrane serves to rapidly distinguish growth and differentiation pattern of normal and malignant human breast epithelial cells, Proc Natl Acad Sci U S A 1992, 89:9064-9068

19. Bissell MJ, Rizki A, Mian IS: Tissue architecture: the ultimate regulator of breast epithelial function, Curr Opin Cell Biol 2003, 15:753-762

20. Efron B, Tibshirani R: An Introduction to the bootstrap. Edited by New York, Chapman & Hall, 1993

21. Birchmeier C, Birchmeier W, Gherardi E, Vande Woude GF: Met, metastasis, motility and more, Nat Rev Mol Cell Biol 2003, 4:915-925

22. Orend G, Chiquet-Ehrismann R: Tenascin-C induced signaling in cancer, Cancer Lett 2006, 244:143-63

23. Boudreau N, Werb Z, Bissell MJA-b: Suppression of apoptosis by basement membrane requires three-dimensional tissue organization and withdrawal from the cell cycle, Proc Natl Acad Sci U S A 1996, 93:3509-3513

24. Tremble P, Chiquet-Ehrismann R, Werb Z: The extracellular matrix ligands fibronectin and tenascin collaborate in regulating collagenase gene expression in fibroblasts, Mol Biol Cell 1994, 5:439-453

25. Tanaka K, Hiraiwa N, Hashimoto H, Yamazaki Y, Kusakabe M: Tenascin-C regulates angiogenesis in tumor through the regulation of vascular endothelial growth factor expression, Int J Cancer 2004, 108:31-40

26. Ioachim E, Charchanti A, Briasoulis E, Karavasilis V, Tsanou H, Arvanitis DL, Agnantis NJ, Pavlidis N: Immunohistochemical expression of extracellular matrix components tenascin, fibronectin, collagen type IV and laminin in breast cancer: their prognostic value and role in tumour invasion and progression, Eur J Cancer 2002, 38:2362-2370

27. Zukiel R, Nowak S, Wyszko E, Rolle K, Gawronska I, Barciszewska MZ, Barciszewski J: Suppression of Human Brain Tumor with Interference RNA Specific for Tenascin-C, Cancer Biol Ther 2006, 5: 1002-1007

28. Reardon DA, Akabani G, Coleman RE, Friedman AH, Friedman HS, Herndon JE, 2nd, McLendon RE, Pegram CN, Provenzale JM, Quinn JA, Rich JN, Vredenburgh JJ, Desjardins A, Gururangan S, Badruddoja M, Dowell JM, Wong TZ, Zhao XG, Zalutsky MR, Bigner DD: Salvage radioimmunotherapy with murine iodine-131-labeled antitenascin monoclonal antibody 81C6 for patients with recurrent primary and metastatic malignant brain tumors: phase II study results, J Clin Oncol 2006, 24:115-122

29. Hicke BJ, Stephens AW, Gould T, Chang YF, Lynott CK, Heil J, Borkowski S, Hilger CS, Cook G, Warren S, Schmidt PG: Tumor targeting by an aptamer, J Nucl Med 2006, 47:668-678

30. Martin TA, Parr C, Davies G, Watkins G, Lane J, Matsumoto K, Nakamura T, Mansel RE, Jiang WG: Growth and angiogenesis of human breast cancer in a nude mouse tumour model is reduced by NK4, a HGF/SF antagonist, Carcinogenesis 2003, 24:1317-1323

31. Jiang WG, Grimshaw D, Martin TA, Davies G, Parr C, Watkins G, Lane J, Abounader R, Laterra J, Mansel RE: Reduction of stromal fibroblast-induced mammary tumor growth, by retroviral ribozyme transgenes to hepatocyte growth factor/scatter factor and its receptor, c-MET, Clin Cancer Res 2003, 9:4274-4281

32. McKean DM, Sisbarro L, Ilic D, Kaplan-Alburquerque N, Nemenoff R, Weiser-Evans M, Kern MJ, Jones PL: FAK induces expression of Prx1 to promote tenascin-C-dependent fibroblast migration, J Cell Biol 2003, 161:393-402

33. Ilic D, Furuta Y, Kanazawa S, Takeda N, Sobue K, Nakatsuji N, Nomura S, Fujimoto J, Okada M, Yamamoto T: Reduced cell motility and enhanced focal adhesion contact formation in cells from FAK-deficient mice, Nature 1995, 377:539-544

34. Matsuda A, Yoshiki A, Tagawa Y, Matsuda H, Kusakabe M: Corneal wound healing in tenascin knockout mouse, Invest Ophthalmol Vis Sci 1999, 40:1071-1080

35. Tucker RP: Abnormal neural crest cell migration after the in vivo knockdown of tenascin-C expression with morpholino antisense oligonucleotides, Dev Dyn 2001, 222:115-119

36. Murphy-Ullrich JE, Lightner VA, Aukhil I, Yan YZ, Erickson HP, Hook M: Focal adhesion integrity is downregulated by the alternatively spliced domain of human tenascin, J Cell Biol 1991, 115:1127-1136

37. Lotz MM, Burdsal CA, Erickson HP, McClay DR: Cell adhesion to fibronectin and tenascin: quantitative measurements of initial binding and subsequent strengthening response, J Cell Biol 1989, 109:1795-1805

38. Koukoulis GK, Howeedy AA, Korhonen M, Virtanen I, Gould VE: Distribution of tenascin, cellular fibronectins and integrins in the normal, hyperplastic and neoplastic breast, J Submicrosc Cytol Pathol 1993, 25:285-295

39. Sarkar S, Nuttall RK, Liu S, Edwards DR, Yong VW: Tenascin-C stimulates glioma cell invasion through matrix metalloproteinase-12, Cancer Res 2006, 66:11771-11780

40. Werb Z, Ashkenas J, MacAuley A, Wiesen JF: Extracellular matrix remodeling as a regulator of stromal-epithelial interactions during mammary gland development, involution and carcinogenesis, Braz J Med Biol Res 1996, 29:1087-1097

41. Duffy MJ: Urokinase plasminogen activator and its inhibitor, PAI-1, as prognostic markers in breast cancer: from pilot to level 1 evidence studies, Clin Chem 2002, 48:1194-1197

42. Jahkola T, Toivonen T, von Smitten K, Virtanen I, Wasenius VM, Blomqvist C: Cathepsin-D, urokinase plasminogen activator and type-1 plasminogen activator

inhibitor in early breast cancer: an immunohistochemical study of prognostic value and relations to tenascin-C and other factors, Br J Cancer 1999, 80:167-174

43. Franz M, Hansen T, Richter P, Borsi L, Bohmer FD, Hyckel P, Schleier P, Katenkamp D, Zardi L, Kosmehl H, Berndt A: Complex formation of the laminin-5 gamma2 chain and large unspliced tenascin-C in oral squamous cell carcinoma in vitro and in situ: implications for sequential modulation of extracellular matrix in the invasive tumor front, Histochem Cell Biol 2006, 126:125-131

44. Niranjan B, Buluwela L, Yant J, Perusinghe N, Atherton A, Phippard D, Dale T, Gusterson B, Kamalati T: HGF/SF: a potent cytokine for mammary growth, morphogenesis and development, Development 1995, 121:2897-2908

45. Peruzzi B, Bottaro DP: Targeting the c-Met signaling pathway in cancer, Clin Cancer Res 2006, 12:3657-3660

46. Beviglia L, Matsumoto K, Lin CS, Ziober BL, Kramer RH: Expression of the c-Met/HGF receptor in human breast carcinoma: correlation with tumor progression, Int J Cancer 1997, 74:301-309

47. Lengyel E, Prechtel D, Resau JH, Gauger K, Welk A, Lindemann K, Salanti G, Richter T, Knudsen B, Vande Woude GF, Harbeck N: C-Met overexpression in node-positive breast cancer identifies patients with poor clinical outcome independent of Her2/neu, Int J Cancer 2005, 113:678-682

48. Soriano JV, Pepper MS, Nakamura T, Orci L, Montesano R: Hepatocyte growth factor stimulates extensive development of branching duct-like structures by cloned mammary gland epithelial cells, J Cell Sci 1995, 108 (Pt 2):413-430

49. Osin PP, Anbazhagan R, Bartkova J, Nathan B, Gusterson BA: Breast development gives insights into breast disease, Histopathology 1998, 33:275-283

50. Wrobel CN, Debnath J, Lin E, Beausoleil S, Roussel MF, Brugge JS: Autocrine CSF-1R activation promotes Src-dependent disruption of mammary epithelial architecture, J Cell Biol 2004, 165:263-273

51. De Wever O, Nguyen QD, Van Hoorde L, Bracke M, Bruyneel E, Gespach C, Mareel M: Tenascin-C and SF/HGF produced by myofibroblasts in vitro provide convergent pro-invasive signals to human colon cancer cells through RhoA and Rac, Faseb J 2004, 18:1016-1018

52. Jones PL, Crack J, Rabinovitch M: Regulation of tenascin-C, a vascular smooth muscle cell survival factor that interacts with the alpha v beta 3 integrin to promote epidermal growth factor receptor phosphorylation and growth, J Cell Biol 1997, 139:279-293

53. Bergstrom JD, Westermark B, Heldin NE: Epidermal growth factor receptor signaling activates met in human anaplastic thyroid carcinoma cells, Exp Cell Res 2000, 259:293-299

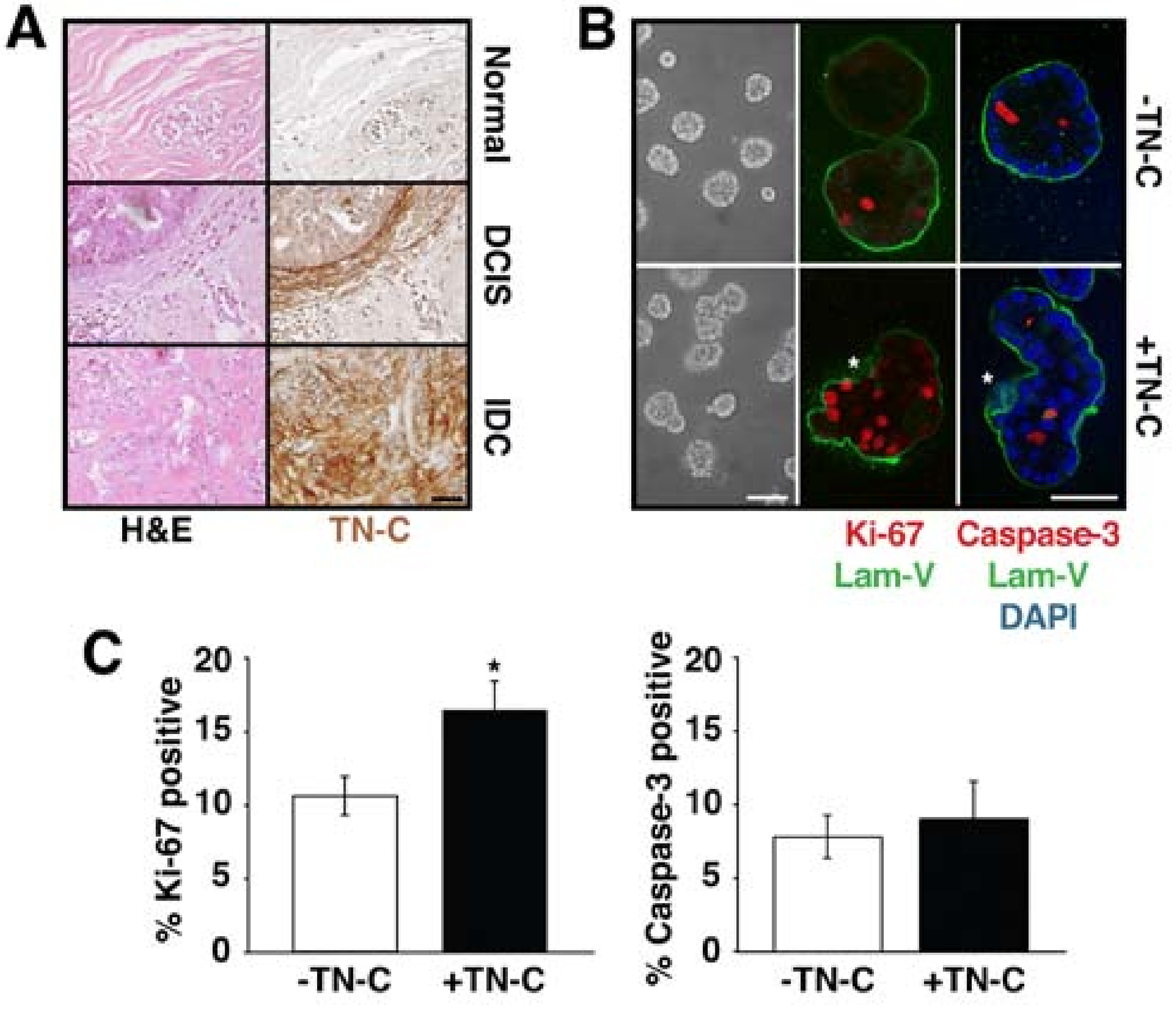
A
Normal
DCIS
IDC
H&E
TN-C
B
-TN-C
+TN-C
Ki-67
Lam-V
Caspase-3
Lam-V
DAPI
C
% Ki-67 positive
20
15
10
5
0
*
-TN-C
+TN-C
% Caspase-3 positive
20
15
10
5
0
-TN-C
+TN-C

Figure 1

A

Capture Z-stacks of Laminin V- or α6 integrin-immunostained 3-D acini

↓

Calculate *dx* & *dy* gradient based on fluorescence intensity

↓

Manually initialize active contours & initiate active contour algorithm

↓

Generate 3-D rendition & compare to best-fitting ellipsoid

↓

Calculate acinar surface roughness & volume

C

B

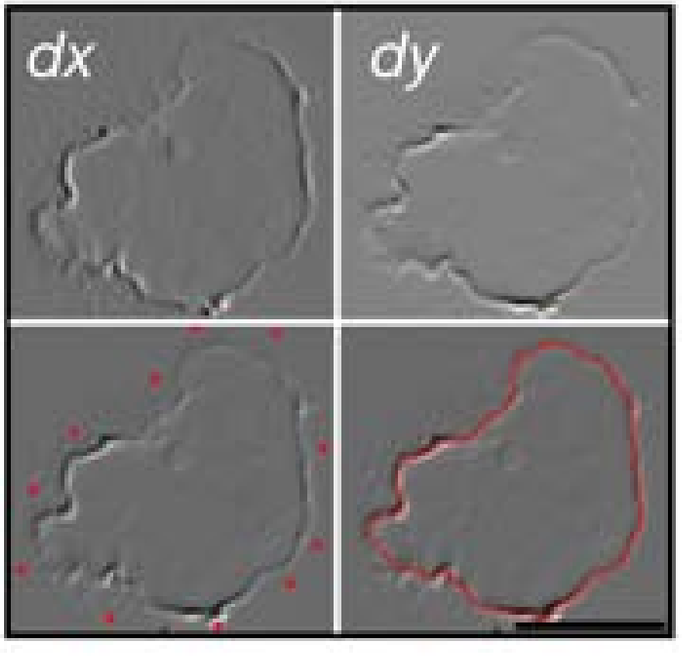

D

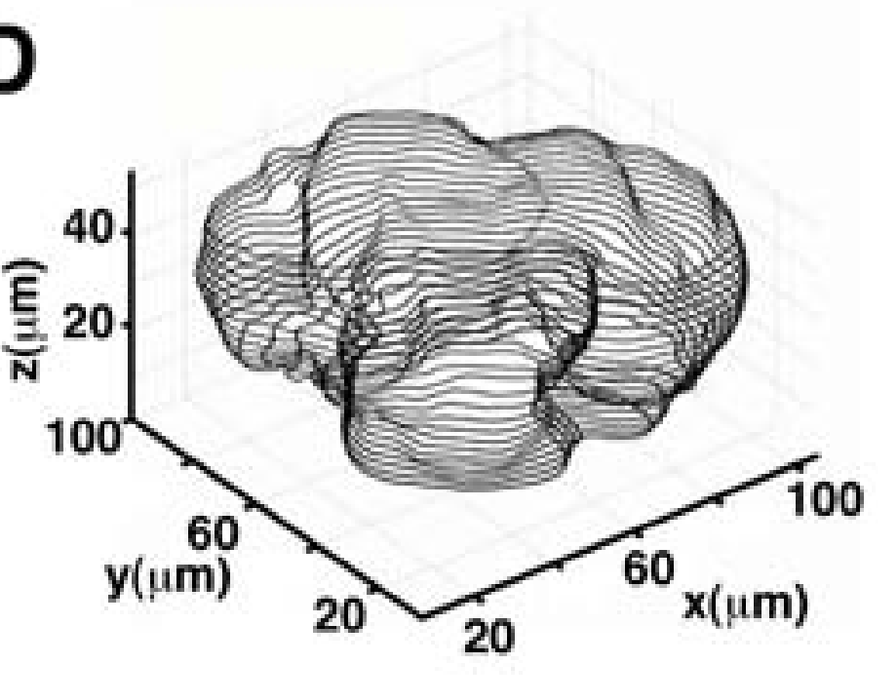

Figure 2

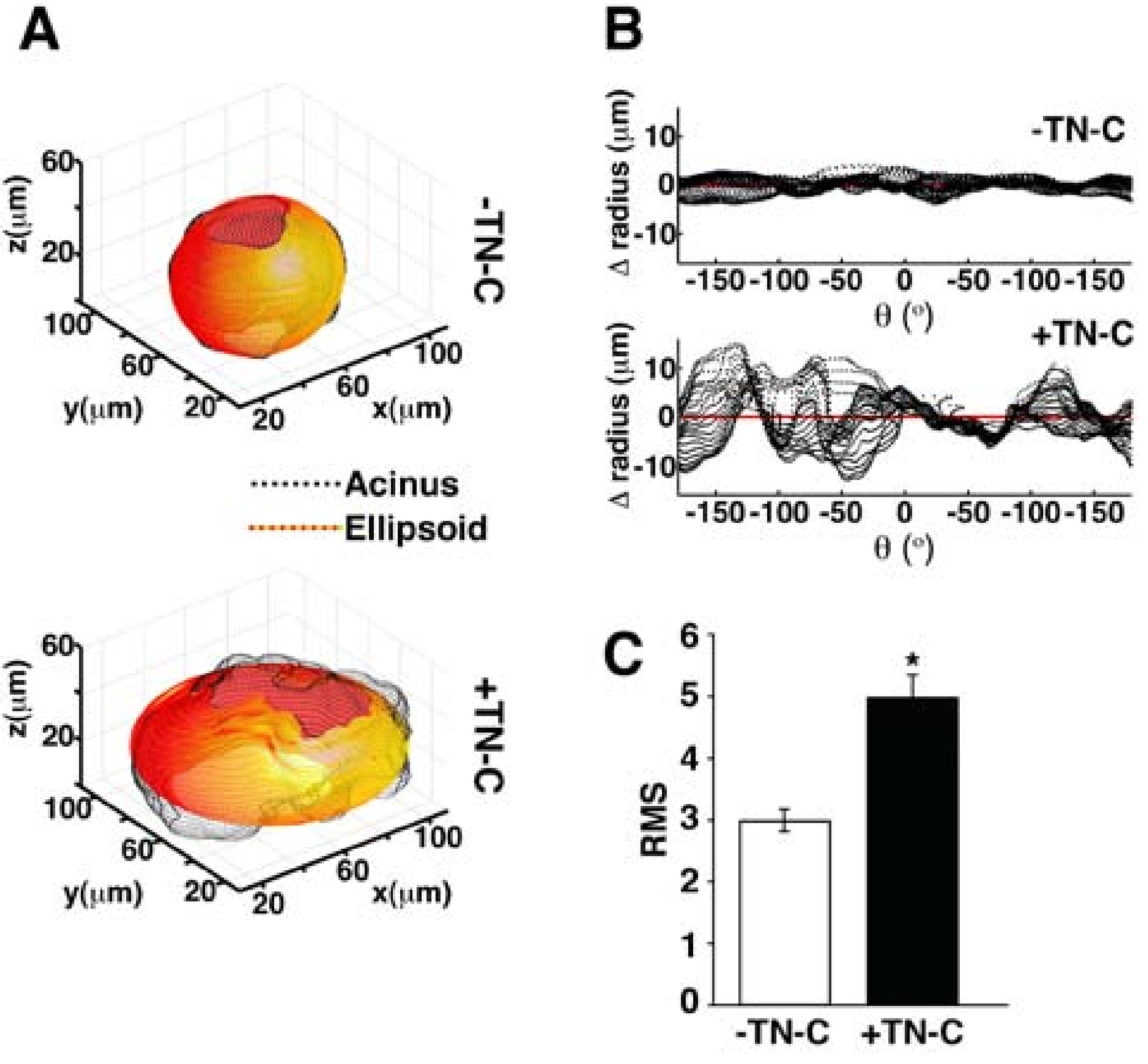
A
-TN-C
z(μm)
y(μm)
x(μm)
Acinus
Ellipsoid
+TN-C
B
-TN-C
+TN-C
Δ radius (μm)
θ (°)
C
RMS
-TN-C
+TN-C

Figure 3

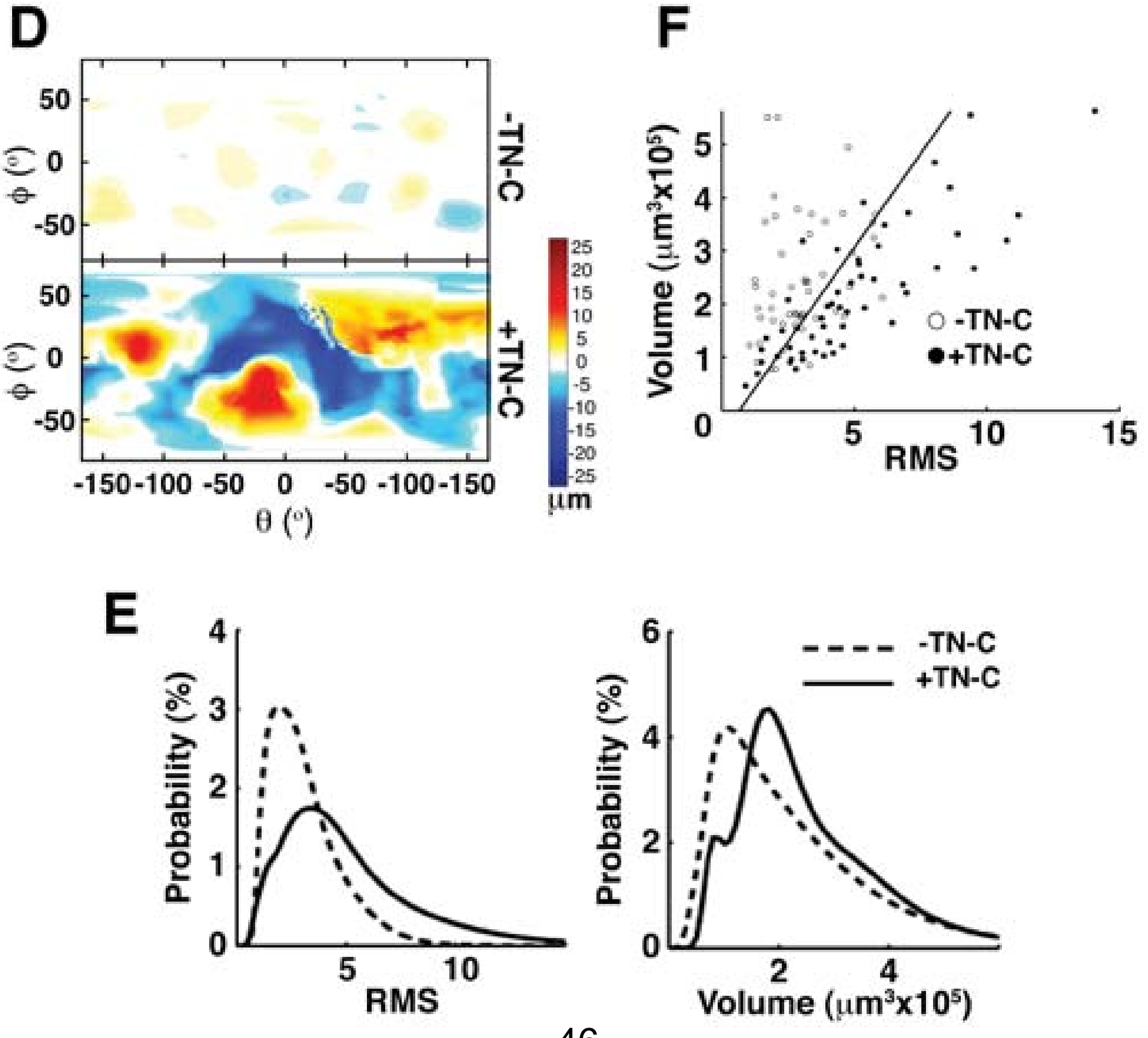
D
50
0
-50
ϕ (°)
-TN-C
+TN-C
-150 -100 -50 0 -50 -100 -150
θ (°)
25
20
15
10
5
0
-5
-10
-15
-20
-25
µm
F
Volume (µm³x10⁵)
RMS
-TN-C
+TN-C
E
Probability (%)
RMS
Volume (µm³x10⁵)
-TN-C
+TN-C

Figure 3

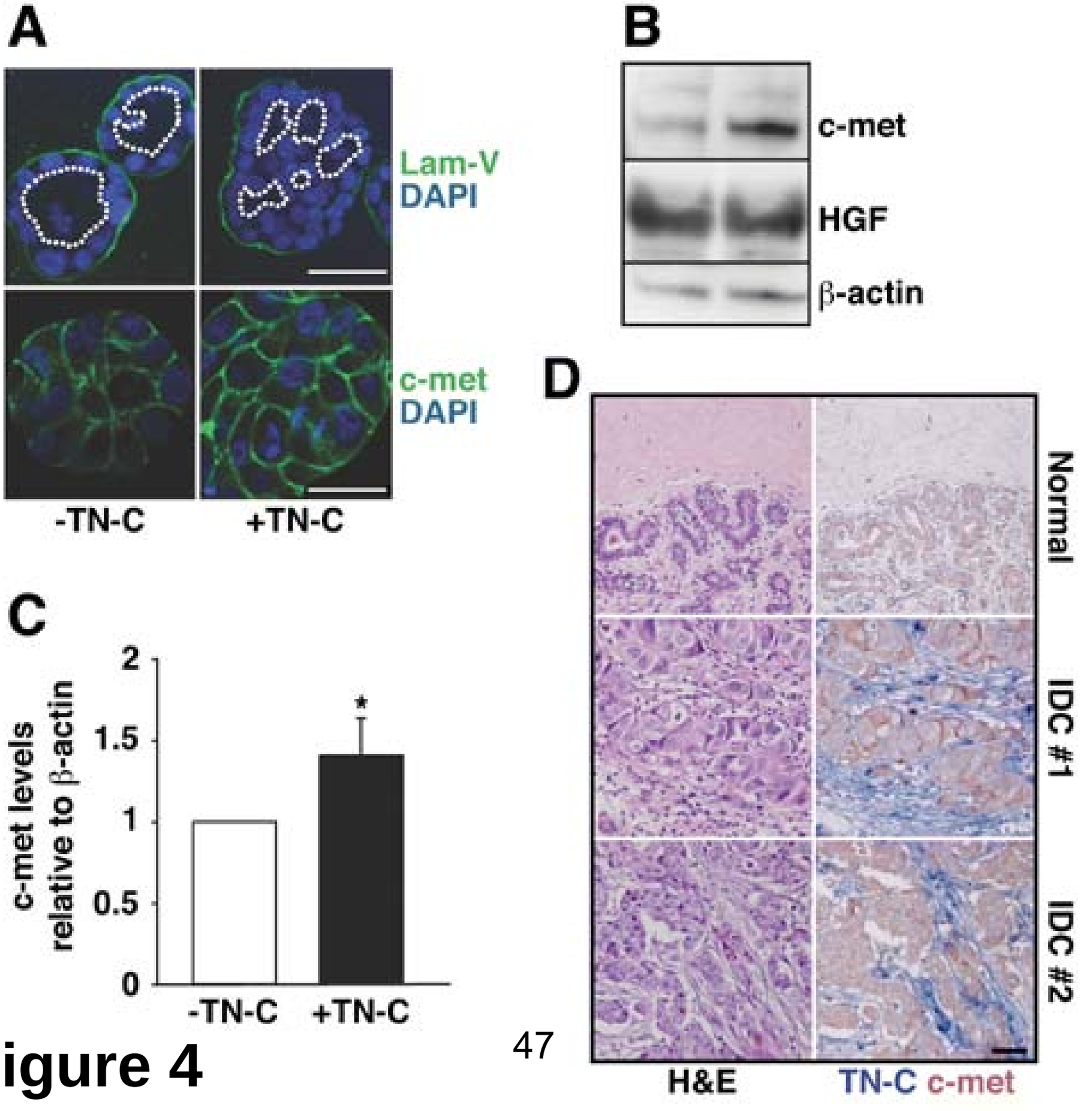
A
Lam-V
DAPI
c-met
DAPI
-TN-C
+TN-C
B
c-met
HGF
β-actin
C
c-met levels
relative to β-actin
2
1.5
1
0.5
0
*
-TN-C
+TN-C
D
Normal
IDC #1
IDC #2
H&E
TN-C c-met

Figure 4

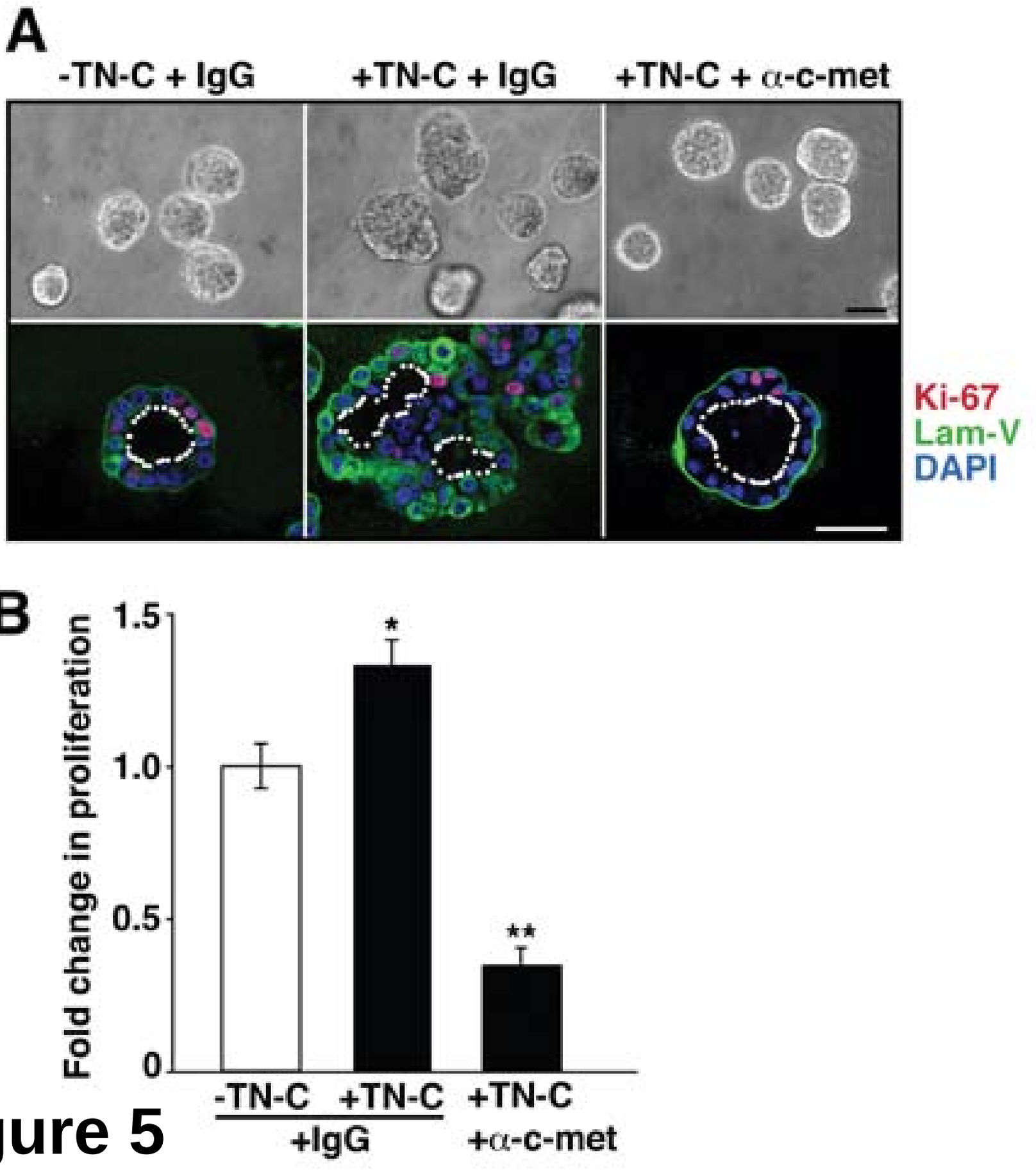
A
-TN-C + IgG
+TN-C + IgG
+TN-C + α-c-met
Ki-67
Lam-V
DAPI
B
Fold change in proliferation
1.5
1.0
0.5
0
*
**
-TN-C
+TN-C
+IgG
+TN-C
+α-c-met

Figure 5

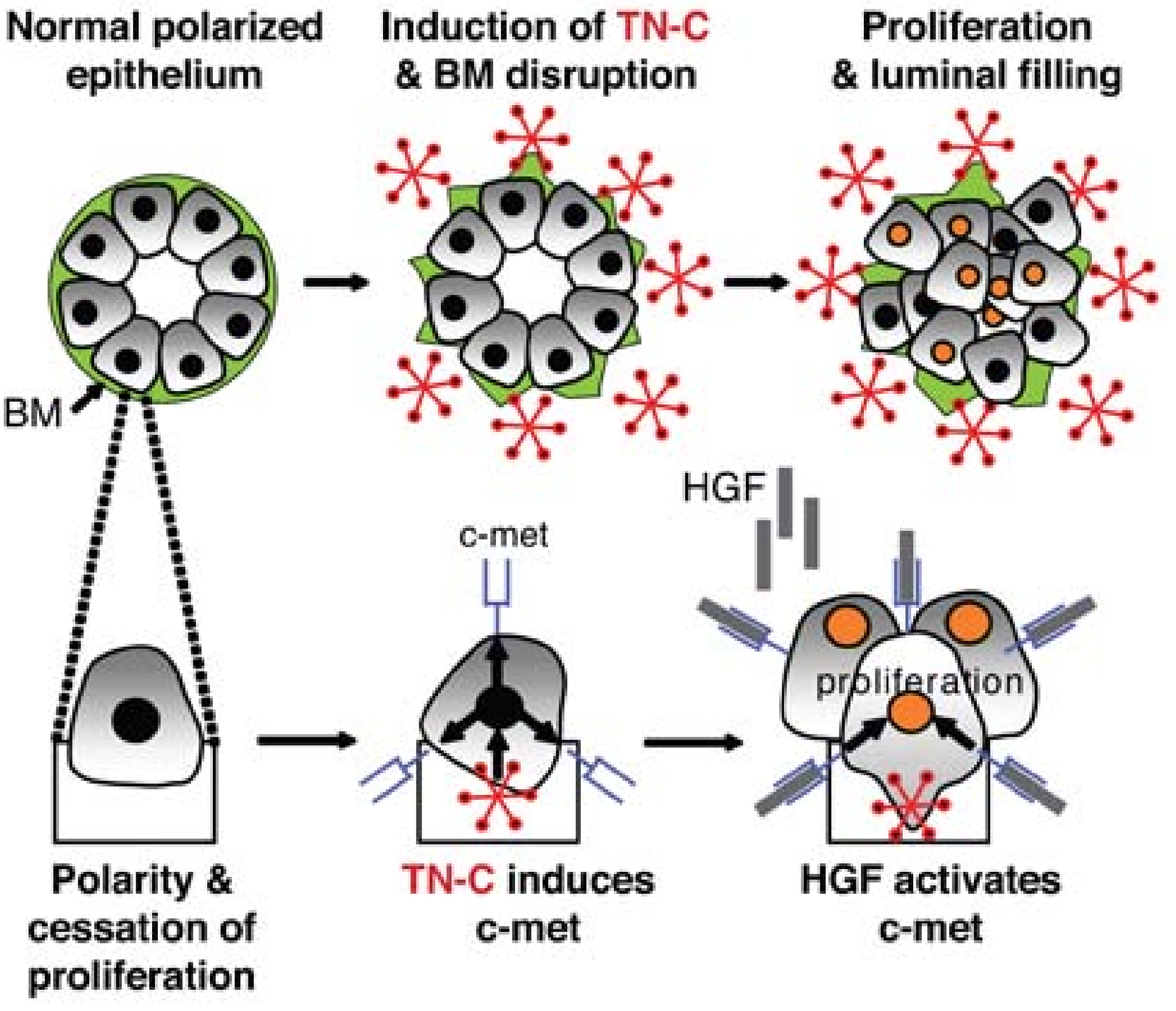
Normal polarized epithelium
Induction of TN-C & BM disruption
Proliferation & luminal filling
BM
HGF
c-met
proliferation
Polarity & cessation of proliferation
TN-C induces c-met
HGF activates c-met

Figure 6